IEEE Photonics Journal
An IEEE Photonics Society Publication

Open Access

Adaptive Target Profile Acquiring Method for Photon Counting 3-D Imaging Lidar

Volume 8, Number 6, December 2016

Ling Ye
Guohua Gu
Weiji He
Huidong Dai
Jie Lin
Qian Chen

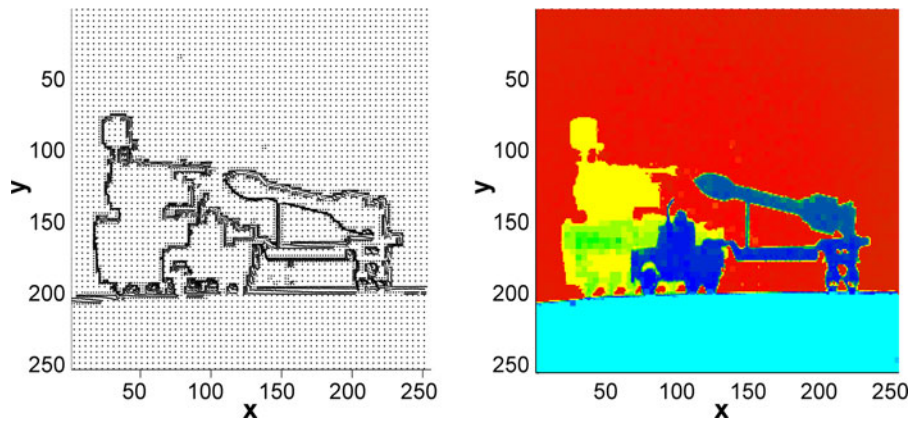

DOI: 10.1109/JPHOT.2016.2625801
1943-0655 © 2016 IEEE

IEEE photonics SOCIETY

IEEE

Adaptive Target Profile Acquiring Method for Photon Counting 3-D Imaging Lidar

Ling Ye,[1] Guohua Gu,[1] Weiji He,[1,2] Huidong Dai,[1] Jie Lin,[1] and Qian Chen[1]

[1]Jiangsu Key Lab of Spectral Imaging and Intelligence Sense, Nanjing University of Science and Technology, Nanjing 210094, China
[2]Key Laboratory of Intelligent Perception and Systems for High-Dimensional Information of the Ministry of Education, Nanjing University of Science and Technology, Nanjing 210094, China

DOI:10.1109/JPHOT.2016.2625801

Manuscript received October 13, 2016; revised November 1, 2016; accepted November 2, 2016. Date of publication November 7, 2016; date of current version November 22, 2016. This work was supported in part by the Seventh Six-Talent Peak Project of Jiangsu Province under Grant 2014-DZXX-007, in part by the National Natural Science Foundation of China under Grant 61271332, in part by the Fundamental Research Funds for the Central Universities under Grant 30920140112012, in part by the Innovation Fund Project for Key Laboratory of Intelligent Perception and Systems for High-Dimensional Information of Ministry of Education under Grant JYC01509, and in part by the Fund Project for Low-Light-Level Night Vision Laboratory under Grant J20130501. Corresponding author: G. Gu (e-mail: gghnjust@163.com).

Abstract: A direct-detection 3-D imaging lidar is capable of acquiring a depth image of noncooperative targets in long distance, using Geiger mode avalanche photodiodes and the technique of time-correlated single-photon counting. However, conventional 3-D imaging lidar has a long data acquisition time. This paper introduces a spatially adaptive method to obtain target profile rapidly for 3-D imaging lidar by exploiting discontinuities between targets and background in the depth domain. The idea behind our strategy is using an adaptive scanning step to localize the regions near the depth boundaries and perform fine scans only to these regions. Fine scans only for those specific regions ensure the recovery accuracy while consuming much less data acquisition time, compared to a conventional high-resolution scanning lidar. Experimental results demonstrate that for the experimental scene, the data acquisition time decreases 85% by using the proposed method, without generating much distortion of the target profile. This method may be of considerable value to fields that need fast 3-D imaging, such as remote sensing and military reconnaissance.

Index Terms: Lidar, 3-D reconstruction, time-of-flight imaging, 3-D imaging, photon counting.

1. Introduction

Three-dimensional (3-D) imaging lidar is widely used to capture the 3-D imaging of the target by illuminating it with pulsed laser and measuring the time-of-flight (TOF) of the back-reflected optical flux [1]–[5]. Moreover, with the use of Geiger mode avalanche photodiodes (GmAPDs) and the technique of time-correlated single-photon counting (TCSPC), the range capacity and measuring accuracy of 3-D imaging lidar have been drastically improved [6], [7].

Many research group constructed imaging lidar systems by adding scanning optics to a single-point lidar systems [8], [9]. For instance, laser pulses are sent out to the scene of interest point-by-point by scanning mechanism while range information is obtained by a single detector. The system

using this scheme is able to obtain depth images with resolutions high enough to identify objects in the range of a kilometer [10], [11]. However, these lidar systems have really long data acquisition time, which limits the real-time performance and lowers the achievable spatial resolution in limited scan time.

In order to deal with this problem, the Lincoln Laboratory at the Massachusetts Institute of Technology [12], [13] proposed to accelerate the imaging process using arrays of detectors. They reported their work on 3-D imaging with 32 $\times$ 32 arrays of GmAPDs which were fully integrated with 32 $\times$ 32 arrays of complementary metal-oxide semiconductor (CMOS) digital timing circuits. Since then, thanks to the development of cost-effective single-chip standard CMOS process, single-photon avalanche diode (SPAD) array cameras have been fabricated to enter the co mmercial market, having a frame-rate up to 100 000 fps and higher spatial resolution. Using these cameras, many fast lidar systems were established to capture the 3-D image of the scene [14]–[21]. Yet these devices are still in their infancy. For currently available SPAD cameras, there are some limitations, such as poor time-tagging performance, high dark count rates and pixel-to-pixel variation of SPAD properties, and result in short range and low depth resolution. On the contrary, the single SPAD detector is mature, which provides stable time-resolved measurements and has lower price.

For lidar systems using an single high-performance SPAD detector, Ahmed Kirmani *et al.* [22] proposed to reduce the data acquisition time by using only the first photon detection at each pixel. They acquired the sub-pulse duration range 3-D structure to exploit the high degree of spatial correlation in real-world scenes. In their work, dwell time per-pixel decreased drastically in first-photon imaging compared to traditional lidar systems. Altmann *et al.* [23] proposed a new Bayesian model to reconstruct a real 3-D object using sparse single-photon data. They obtained excellent experimental results with respect to reducing per-pixel acquisition time to sub-millisecond, while conventional methods need more than tenfold time. Recently, a novel lidar architecture utilizing single-pixel detectors was proposed. This framework operates with short acquisition time [24].

Here, we proposed a spatially non-uniform scanning method to reduce the amount of unnecessary scanning points in order to reduce the data acquisition time. For most targets of interest in natural scene, the ranges of the targets surface areas have small total variation due to the characteristic of the surface continuity. Thus there is compressibility in the depth gradient domain which we can exploit to reduce the amount of scanning points for reconstruction. Meanwhile, the boundaries of different targets or different parts of targets always bring a depth-variation over a certain threshold. For the raster-scanning process of lidar, the temporal difference of the echo signals on adjacent pixels can be analyzed to locate the depth boundaries of targets and finer scans are performed to these regions to reconstruct accurate 3-D images of the targets. Because the proposed method is spatially-adaptive and has high efficiency in reducing data acquisition time for different scenes, it paves the way for fast lidar systems in applications such as 3-D biological imaging of ultrafast processes, dynamic imaging for airborne remote sensing and military object identification in a long range.

2. Working principle

2.1. Conventional method

Since laser spots has a small size compared to the target distance and the scene is composed of locally continuous surfaces, it was a reasonable assumption that the laser spot associated with a given pixel is incident on a single surface. Due to the fixed scanning step length in conventional methods, scanning points are uniformly distributed in scanning field of view (SFOV). If the resolution of scanning points is not high enough, it will lead to loss of details of the target profile.

Here we use a simple scene (see Fig. 1) to illustrate the generation of distortion of the depth image. The scene contains a flat foreground target and a clean background, which means it should have two depth values in its depth image, as shown in Fig. 1(a). We assume that the target has a 10 cm depth difference with the background. A 3 $\times$ 3 fixed scanning grid is performed in the scene using the conventional scanning method, dividing the scene into 3 $\times$ 3 pixels (the relative position

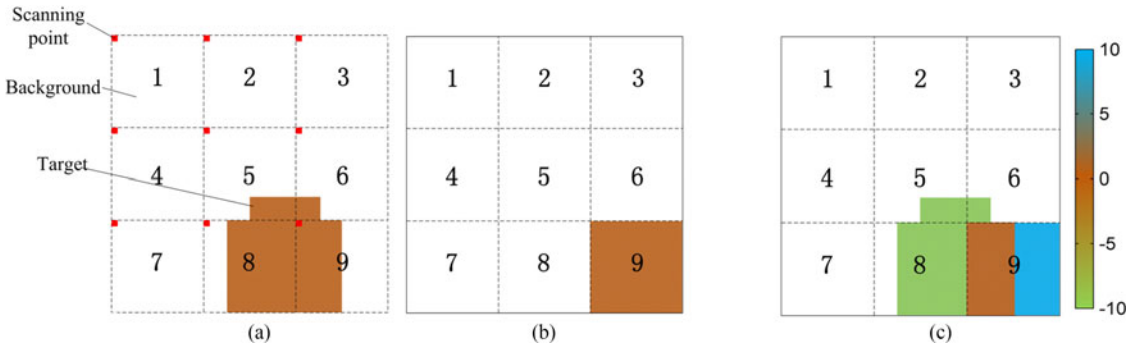

Fig. 1. (a) Simple scene to illustrate how conventional method loses details of depth profile. (b) Depth reconstructed result of conventional method using a 3 × 3 fixed scanning grid. (c) Error map calculated by Fig. 1(a) and (b) in depth domain.

of the exact scanning point in the corresponding pixel does not influences the image result). The depth value of each pixel is determined by TOF of the only scanning point on this pixel. By collecting the TOF information of all pixels, a depth image of the SFOV can be estimated.

Fig. 1(b) shows the reconstructed depth image of the scene. It can be seen that the result loses many details of the target profile. Low-resolution scanning grid makes a single divided pixel cover too large area which may include several depth value, such as pixel 5, 6, 8, and 9. This kind of pixels we call them multi-depth pixels. These multi-depth pixels are assigned by the single depth value of the only scanning point associated with the corresponding pixel, which in all probability lead to distortion, as shown in an error map calculated by Fig. 1(a) and Fig. 1(b) in depth domain, and Fig. 1(c). (For viewing convenience, most areas of background are not color-coded.) The brown part in Fig. 1(c) represents accurate reconstruction of the target. The green part and the blue part represent the areas of underestimation and overestimation of depths, respectively.

As can be seen from the illustration above, the existence of multi-depth pixels generates distortions of the target profile in low-resolution scans. Shortening fixed scanning step length to reach higher resolution can reduce the amount of multi-depth pixels and improve the accuracy of target profile in depth image. However, short fixed scanning step length will lead to dramatic increase of scanning points because conventional method has a uniform distribution of scanning points and is inefficient to acquire depth profile, which will bring redundant data and slow down imaging speed.

2.2. Proposed method

Since there exists the contradiction between the accuracy and speed in conventional scanning methods for raster-scanning lidar, a spatially-adaptive scanning method is proposed. In our method, low-resolution scans are used to acquire depth information rapidly due to the compressibility in depth domain of natural scenes. Then fine scans are performed to the specific regions only to eliminate multi-depth pixels located by algorithm.

Firstly, a big-foot scanning for an initial profile estimation divides SFOV into $m \times n$ pixels. Depth value measured by TOF of scanning points incident on the pixel at i-th line j-th column is denoted as $D\,i, j$. A $m \times n$ matrix with initial value 0 is denoted as Φ, determined as follows:

$$\begin{aligned}
&\text{IF} \quad \left|D_{i,j} - D_{i+1,j}\right| \geq T \quad \text{THEN} \quad \Phi(i,j) = \Phi(i+1,j) = 1 \\
&\text{IF} \quad \left|D_{i,j} - D_{i,j+1}\right| \geq T \quad \text{THEN} \quad \Phi(i,j) = \Phi(i,j+1) = 1 \\
&\text{IF} \quad \left|D_{i,j} - D_{i+1,j+1}\right| \geq T \quad \text{THEN} \quad \Phi(i,j) = \Phi(i+1,j+1) = 1 \\
&\text{ELSE IF} \quad \left|D_{i,j} - D_{i+1,j}\right| < T \;\&\; \left|D_{i,j} - D_{i,j+1}\right| < T \;\&\; \left|D_{i,j} - D_{i+1,j+1}\right| < T \\
&\text{THEN} \quad \Phi(i,j) < -\Phi(i,j)
\end{aligned} \tag{1}$$

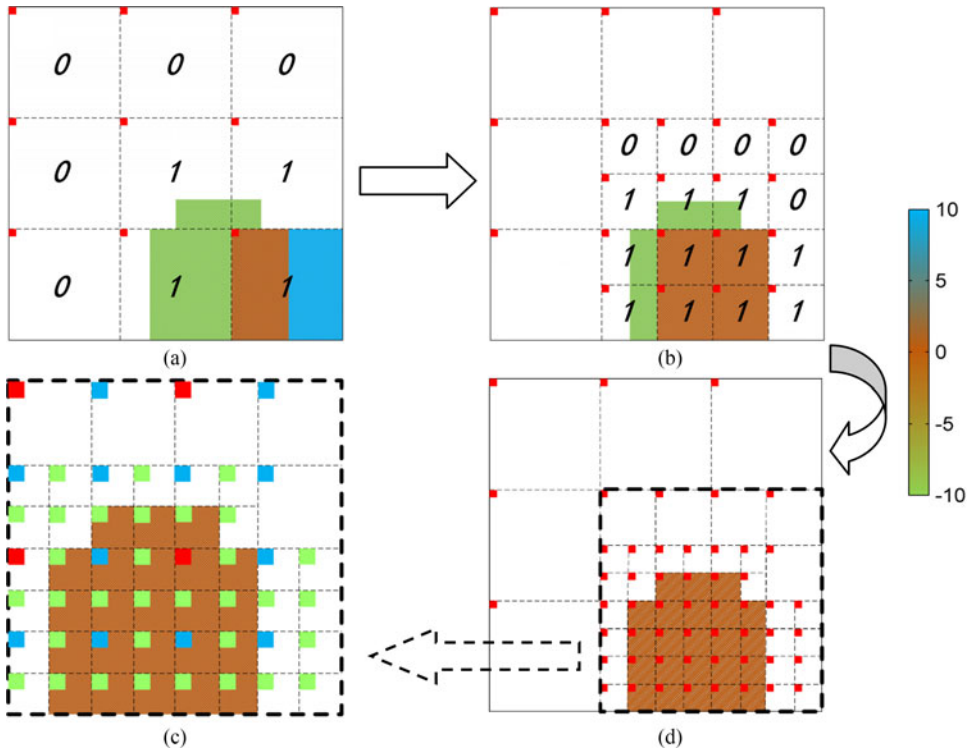

Fig. 2. (a)–(c) Diagrammatic flow chart of our method. (d) Distribution of laser spots in these three scans.

where $i \leq m-1$, $j \leq n-1$, and T is the threshold to judge whether there is a depth hop between two adjacent pixels. If $\Phi(i, j) = 0$, pixel (i, j) only has a single depth. Otherwise, the corresponding pixel is likely to be a multi-depth pixel and will be performed a finer scan.

Based on the value of Φ, pixels near the target profile which are potential to be multi-depth pixels are distinguished. As shown in Fig. 2(a) and Fig. 2(b) (For viewing convenience, targets are color-coded as Fig. 1(c).), only the potential multi-depth pixels are divided into 2×2 sub-pixels after a fine scan. All of the sub-pixels form the second-stage depth image to supplement the initial image. Similarly, the second-stage depth image is calculated by (1) to generate a new dual-value matrix Φ' to judge that which pixel in the second-stage depth image needs a finer scan. Then next stage depth image is obtained. Finally, after several similar procedures above, several supplemental depth images are obtained to constitute a final depth image. Fig. 2(c) illustrates the final depth image constituted by the initial depth image and two supplemental depth images. Fig. 2(d) shows how scanning points in these three scans are distributed. Red spots represent the scanning points from the first scanning. Blue and Green spots symbolize the scanning points from the second-stage image and third-stage depth image, respectively.

From Fig. 2 and (1), it can be seen that the proposed method eliminates multi-depth pixels effectively by increasing the local resolution near the target profile, rather than simply increasing the general resolution. The fine scans for specific regions lead to the proposed method acquire the target profile rapidly while having a small deterioration in the recovery accuracy.

The threshold T determines whether a multi-depth pixel exists, that is, whether there is a discernible hop in the depth domain between two adjacent scanning points. Thus, selection of the threshold T should consider the system timing jitter Δt_{system}.

Each component in the system contributes to Δt_{system}, which can be represented as in [25]

$$\Delta t_{system} = \sqrt{\Delta t_{TCSPC}^2 + \Delta t_{SPAD}^2 + \Delta t_{Laser}^2 + \Delta t_{SYNC}^2}$$

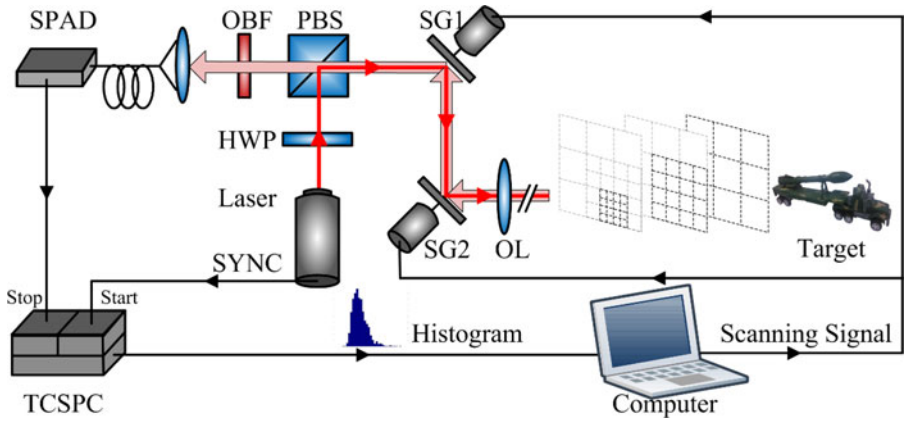

Fig. 3. Schematic of the experimental setup. SPAD, single-photon avalanche diode; OBF, optical band-pass filter; PBS, polarization beam splitter; HWP, half-wave plate; SG1 and SG2, scanning galvo; OL, objective lens; SYNC, synchronous trigger signal of the laser source.

where Δt_{TCSPC}, Δt_{SPAD}, Δt_{Laser}, and Δt_{SYNC} represent timing jitters from the TCSPC module, the SPAD module, the laser, and the synchronization signal of the laser, respectively.

In order to determine whether there is a hop in the depth domain, the threshold T should be larger than the depth resolution of the system, $\Delta R = \Delta t_{system} \bullet c/2$. The exact value of T is determined by the particular scene and limitation of scanning time.

3. Experimental setup

As shown in Fig. 3, an experimental setup is established for the feasibility test of our method. A pulsed laser diode (PicoQuant GmbH, PDL800-B) is used as the photon source. 830-nm wavelength laser pulses with a full width at half maximum (FWHM) of 70 ps are emitted through a half-wave plate (HWP) at a repetition rate of 2.5 MHz. The optical transceiving system is operated in coaxial output mode through a half-wave plate (HWP) and a polarization beam splitter (PBS). The transmitted laser pulse is directed to some point in SFOV by a 2-axis scanning galvo system (Thorlabs, GVS002, small angle step response 300 μs) controlled by a computer. A commercial lens of single-lens reflex camera (Nikon, 200 mm, f/2.8) is used as the objective lens (OL) of the system, collecting as many reflected photons as possible.

After the background noise being blocked by an optical bandpass-filter (OBF), of which band width is 12 nm and peak transmittance is 55% in the 830 nm working wavelength, the return photons are coupled into a SPAD (PerkinElmer, SPCM-AQR-14, dead time 50 ns, dark count 50 Hz, timing jitter 350 ps) through a fiber. The output of the SPAD is connected to “Stop” of the TCSPC (PicoHarp300, PicoQuant GmbH, Germany) while the synchronizing signal from laser diode is connected to “Start”. The TOF histogram of reflected light acquired by TCSPC with a 4-ps resolution is sent to the computer to reconstruct the depth imaging. For the fixed dwell time of 10 ms, the average total number of photons detected by SPAD per scanning point is $\sim$6000. The noise count from background noise and dark count is $\sim$5 kHz, measured when the laser source is power-off.

All the components are upon the optimal selection that can be afforded and they are all optimized to decrease their jitters. In this system, Δt_{system} is 351 ps (Δt_{TCSPC}= 12 ps, Δt_{SPAD}= 350 ps, Δt_{Laser}= 2.6 ps, Δt_{SYNC}= 20 ps), and $\Delta R = \Delta t_{system} \bullet c/2$ is 52.65 mm.

4. Experimental results and analysis

The targets and experimental results are shown in figures below. The imaged targets are shown in Fig. 4(a), in which the dash box is the scanning area. The relative positions of these models are shown in Fig. 4(b). The targets are placed at a range of $\sim$21 m from the imaging setup.

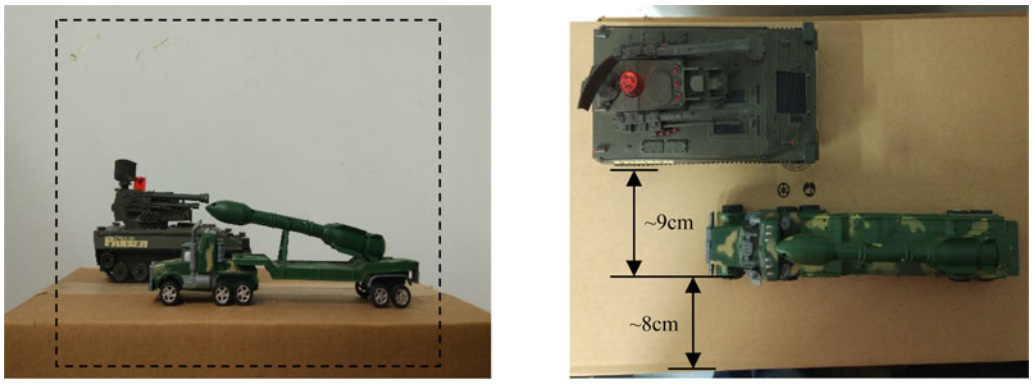

Fig. 4. Imaged targets: a missile launcher model and a panzer model. (a) Scanned scene. (b) Relative positions of the targets.

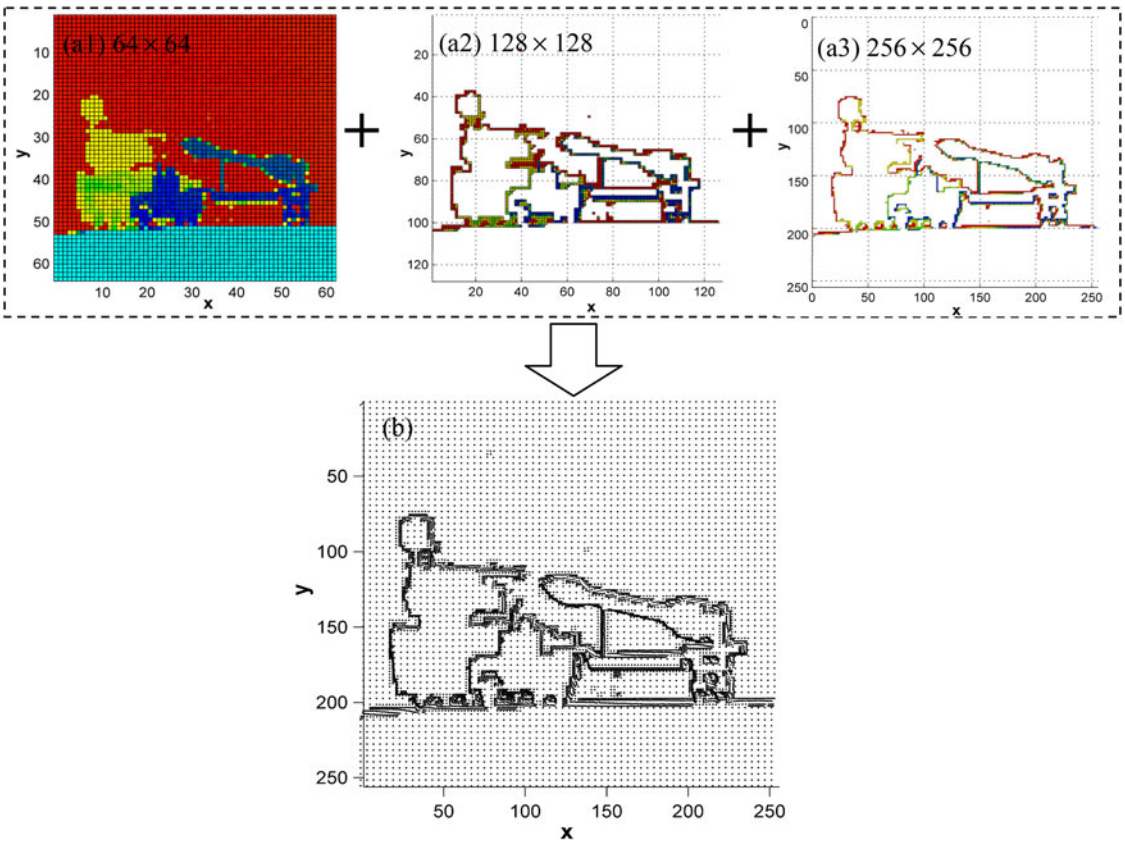

Fig. 5. Experimental results. (a1)–(a3) Initial depth image and two supplemental depth image. (b) Distribution of laser spots in final depth image of our method.

A straightforward approach is implemented to get a depth value at a pixel from the raw TCSPC histogram: the final depth value from the raw TCSPC histogram is determined by its centroid. The experimental results are shown in Fig. 5 and Fig. 6. The depth image results that exploit the proposed method are acquired by three sub-sampling scans and the equivalent resolutions respectively are 64 × 64, 128 × 128 and 256 × 256, as shown in Fig. 5(a1), (a2), and (a3). Among them, scanning points in Fig. 5(a1) are uniformly distributed, while Fig. 5(a2) and (a3) only have

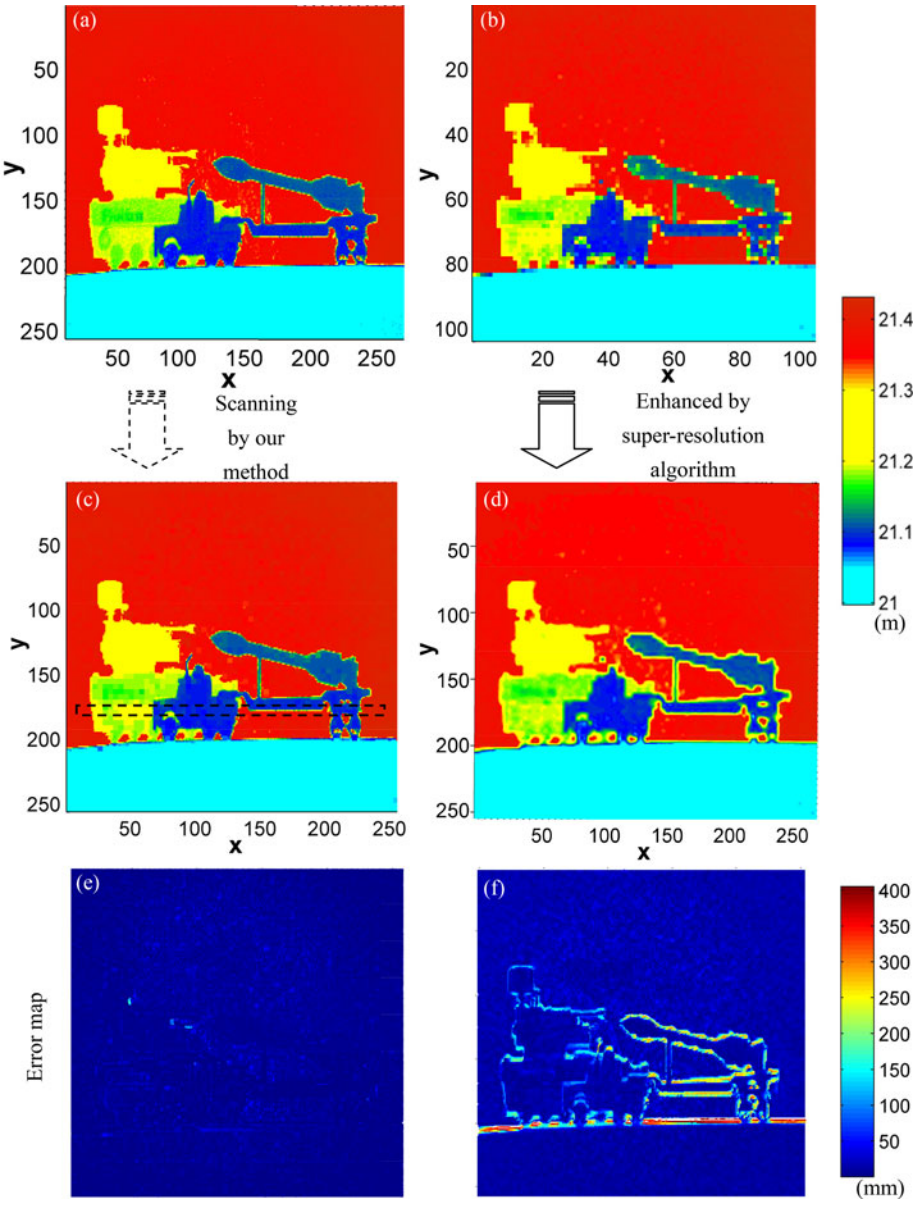

Fig. 6. (a) Depth image of the ground truth using conventional method with 256 × 256 pixels. (b) Depth image of conventional method with 100 × 100 pixels. (c) Depth image using our method. (d) Depth image enhanced to 256 × 256 pixels from Fig. 6(c) using bicubic interpolation super-resolution algorithm. (e) Error map between Fig. 6(a) and (c). (f) Error map between Fig. 6(a) and (d).

scanning points on marked pixels. Results from these three sub-sampling scans form the final depth image of our method. Fig. 5(b) shows how the scanning points in the final depth image of our method are distributed. It can be seen that most of the points are concentrated near the target profile where depth gets a hop and multi-depth pixels possibly exist. The amount of scanning points in Fig. 5(b) is 9559 and the highest local resolution is 256 × 256.

A 256 × 256 pixels depth image using the conventional point-by-point approach is considered as the ground truth image, as shown in Fig. 6(a). Two depth images that contain a similar number of scanning points are shown in Fig. 6(b) and (c). Fig. 6(b) is 100 × 100 pixels and acquired by conventional method. Fig. 6(c) shows the result of our method, of which scanning points have a spatially non-uniform distribution and the highest local resolution is 256 × 256. The numbers of

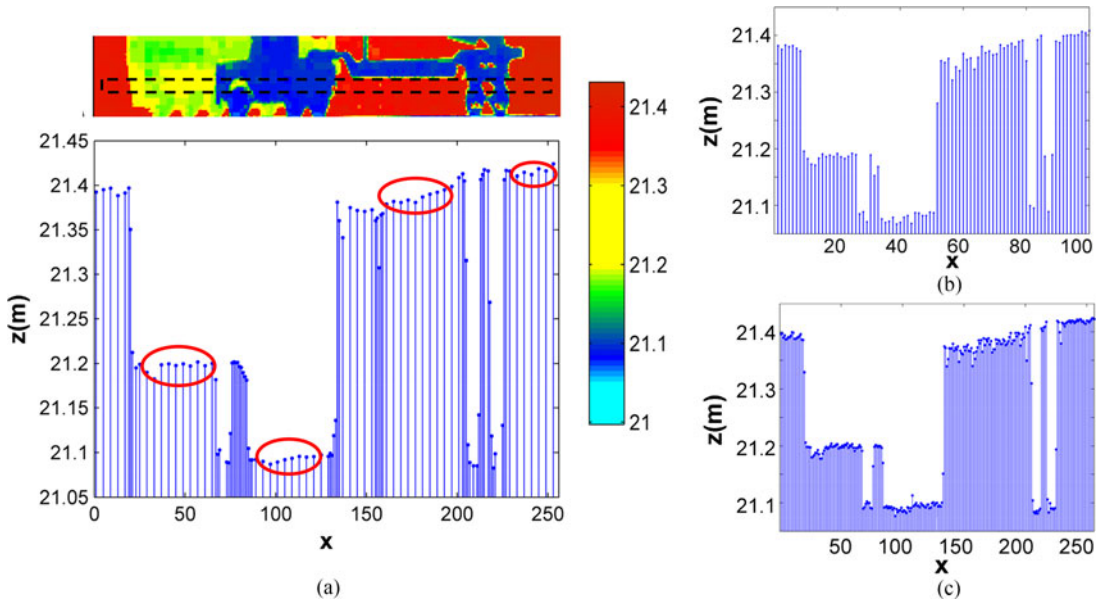

Fig. 7. (a) Plots of depth values of line 181 in Fig. 5(c): the final depth image of our method. (b) Plots of depth values of line 181 in Fig. 5(d): depth image of conventional method with 256 × 256 pixels. (c) Plots of depth values of line 71 in Fig. 5(e): depth image of conventional method with 100 × 100 pixels.

scanning points are 9559, 15% of the ground truth image. Compared to Fig. 6(b), the result of our method has a clearer depth profile of targets with more details. In order to make a further evaluation of the proposed method, we use a super-resolution algorithm (Bicubic interpolation, MATLAB) to enhance Fig. 6(b) to 256 × 256 pixels, as shown in Fig. 6(d). The result of the conventional method has been improved due to higher resolution. However, the super-resolution software cannot recover the lost details and fails to super-resolve the regions of depth boundaries correctly due to the existence of multi-depth pixels, especially in regions with fine spatial features, such as regions near tires, vehicle vent-pipe and missile rudder. Hence, there are high values near the regions of depth boundaries in the error map between the super-resolved image and the ground truth image, as shown in Fig. 6(f), while Fig. 6(e) has few high values. Based on Fig. 6(a), the ground truth image, the RMSE of the super-resolved result using the conventional method is 42.5401 mm, while the root mean square error (RMSE) of the proposed method has decreased to 8.1764 mm using even fewer scanning points.

Fig. 7(a) shows the depth values of line 181 in Fig. 6(b) which is marked in the dashed rectangle, while Fig. 7(b) and 7(c) show the depth values of the corresponding parts in Fig. 6(a) and (c), respectively. From Fig. 7(a), it can been seen the proposed method reduces unnecessary scanning points where the surface is continuous, as shown in red cycle in Fig. 7(a). The target profile keeps integrity because the proposed method has the sensitivity to depth changes which will lead to high local resolution near the target profile. Compared to the proposed method, scanning points in Fig. 7(b) are uniformly distributed and not enough near the profile of targets. Low-resolution scans performed to multi-depth pixels will lead to the distortion of target profile. Shortening fixed scanning step length can improve resolution and increase details of the target profile, as shown in Fig. 7(c); however, its insensitiveness to depth changes leads to the significant increase of the amount of scanning points, making this approach inefficient.

In order to quantify the effect of the proposed method, the RMSE values of the proposed method and the conventional method are represented as color plots in Fig. 8. The 256 × 256 pixels depth image using the conventional point-by-point approach with a fixed scanning step length (see Fig. 6(a)) is considered to be the ground truth. The results of the conventional method are enhanced to 256 × 256 pixels by super-resolution algorithm (bicubic interpolation) in order to calculate the

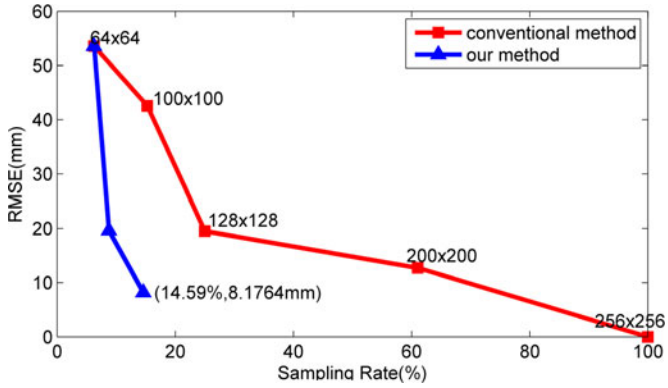

Fig. 8. Plots of RMSE versus sampling rate, blue plots: our method, red plots: conventional method with a fixed scanning grid.

RMSE. It can be seen that the RMSE values of the conventional method decline slowly with the increase of the sampling rate (the number of scanning points of the image divided by the number of scanning points in the ground truth image) while the RMSE values of our method decline fast in a low sampling rate.

The high efficiency of our method benefits from exploiting the compressibility in near-flat regions and the low RMSE benefits from the high-resolution scans performed to regions of depth boundaries.

5. Conclusion

In this paper, a heuristic method that can rapidly obtain depth profile of unknown targets is presented. Exploiting discontinuity of targets and background in the depth domain, regions near the target profile are localized to perform fine scans. In our spatially-adaptive scanning method, scanning points concentrate near the target profile to eliminate multi-depth pixels. Compared to the conventional method using a fixed scanning grid, the proposed method consumes much less data acquisition time to obtain a clear depth profile of targets efficiently. For the experimental scene, the results demonstrate that the proposed method reduces 85% data acquisition time of the conventional method while only having a small deterioration in the recovery accuracy. This high efficient method is significant for fields which have the needs to obtain profile of unknown targets, especially for military applications. For searching and recognizing unknown targets, the SFOV tend to be set large and the proposed method will have a better performance due to more regions of small depth variation.

In the experimental system, the main source of timing jitter is from the SPAD. By using low-jitter detector, such as superconducting nanowire single-photon detector (SNSPD) [26]–[30], timing jitter of the system will be reduced significantly and the proposed method can get a smaller threshold T and a richer depth hierarchy.

In this paper, we use a 2×2 neighborhood to compute depth boundary map. In future works we will study different methods for locating the depth boundaries and exploiting the intensity information to increase the robustness. Additionally, we will analyze how the RMSE value changes with varying SNR of experiments.

References

[1] B. Schwarz, "Mapping the world in 3D," *Nature Photon.*, vol. 4, no. 7, pp. 429–430, 2010.
[2] R. M. Marino and W. R. Davis, "Jigsaw: A foliage-penetrating 3D imaging laser radar system," *Lincoln Lab. J.*, vol. 15, no. 1, pp. 23–36, 2005.

[3] M. Danesh Panah, B. Javidi, and E. A. Watson, "Three dimensional object recognition with photon counting imagery in the presence of noise," *Opt. Exp.*, vol. 18, no. 25, pp. 26450–26460, 2010.
[4] A. Maccarone *et al.*, "Underwater depth imaging using time-correlated single-photon counting," *Opt. Exp.*, vol. 23, no. 26, pp. 33911–33926, 2015.
[5] D. Shin, A. Kirmani, V. K. Goyal, and J. H. Shapiro, "Photon-efficient computational 3-D and reflectivity imaging with single-photon detectors," *IEEE Trans. Comput. Imag.*, vol. 1, no. 2, pp. 112–125, Jun. 2015.
[6] D. G. Fouche, "Detection and false-alarm probabilities for laser radars that use Geiger-mode detectors," *Appl. Opt.*, vol. 42, no. 27, pp. 5388–5398, 2003.
[7] J. S. Massa, A. M. Wallace, G. S. Buller, S. J. Fancey, and A. C. Walker, "Laser depth measurement based on time-correlated single-photon counting," *Opt. Lett.*, vol. 22, no. 8, pp. 543–545, 1997.
[8] G. Buller and A. Wallace, "Ranging and three-dimensional imaging using time-correlated single-photon counting and point-by-point acquisition," *IEEE J. Sel. Topics Quantum Electron.*, vol. 13, no. 4, pp. 1006–1015, Jul./Aug. 2007.
[9] L. Sjöqvist, M. Henriksson, P. Jonsson, and O. Steinvall, "Time-correlated single-photon counting range profiling and reflectance tomographic imaging," *Adv. Opt. Technol.*, vol. 3, no. 2, pp. 187–197, 2014.
[10] A. McCarthy *et al.,* "Kilometer-range depth imaging at 1550 nm wavelength using an InGaAs/InP single-photon avalanche diode detector," *Opt. Exp.*, vol. 21, no. 19, pp. 22098–22113, 2013.
[11] A. McCarthy *et al.*, "Kilometer-range, high resolution depth imaging via 1560 nm wavelength single-photon detection," *Opt. Exp.*, vol. 21, no. 7, pp. 8904–8915, 2013.
[12] B. F. Aull *et al.*, "Geiger-mode avalanche photodiodes for three-dimensional imaging," *Lincoln Lab. J.*, vol. 13, no. 2, pp. 335–349, 2002.
[13] M. A. Albota *et al.*, "Three-dimensional imaging laser radars with Geiger-mode avalanche photodiode arrays," *Lincoln Lab. J.*, vol. 13, no. 2, pp. 351–370, 2002.
[14] C. Niclass and E. Charbon, "A single photon detector array with 64 $\times$ 64 resolution and millimetric depth accuracy for 3D imaging," in *Proc. IEEE Int. Solid-State Circuits Conf. Dig. Tech. Papers*, Feb. 2005, pp. 364–604.
[15] J. Richardson *et al.*, "A 32 $\times$ 32 50 ps resolution 10 bit time to digital converter array in 130 nm CMOS for time correlated imaging," in *Proc. IEEE Custom Integr. Circuits Conf.*, Sep. 2009, pp. 77–80.
[16] M. Entwistle *et al.*, "Geiger-mode APD camera system for single-photon 3D LADAR imaging," *Proc. SPIE*, May 2012, Art. no. 83750D.
[17] D. Bronzi *et al.*, "100 000 frames/s 64 $\times$ 32 single-photon detector array for 2-D imaging and 3-D ranging," *IEEE J. Sel. Topics Quantum Electron.*, vol. 20, no. 6, pp. 354–363, Nov./Dec. 2014.
[18] F. Villa *et al.*, "CMOS imager with 1024 SPADs and TDCs for single-photon timing and 3-D time-of-flight," *IEEE J. Sel. Topics Quantum Electron.*, vol. 20, no. 6, pp. 364–373, Nov./Dec. 2014.
[19] R. Lussana, F. Villa, A. Dalla Mora, D. Contini, A. Tosi, and F. Zappa, "Enhanced single-photon time-of-flight 3D ranging," *Opt. Exp.*, vol. 23, no. 19, pp. 24962–24973, 2015.
[20] D. Bronzi, Y. Zou, F. Villa, S. Tisa, A. Tosi, and F. Zappa, "Automotive three-dimensional vision through a single-photon counting SPAD camera," *IEEE Trans. Intell. Transp. Syst.*, vol. 17, no. 3, pp. 782–795, 2016.
[21] D. Shin *et al.*, "Photon-efficient imaging with a single-photon camera," *Nature Commun.*, vol. 7, 2016, Art. no. 12046.
[22] A. Kirmani *et al.*, "First-photon imaging," *Science*, vol. 343, no. 6166, pp. 58–61, 2014.
[23] Y. Altmann, X. Ren, A. McCarthy, G. S. Buller, and S. McLaughlin, "Lidar waveform-based analysis of depth images constructed using sparse single-photon data," *IEEE Trans. Image Process.*, vol. 25, no. 5, pp. 1935–1946, May 2016.
[24] M. J. Sun *et al.*, "Single-pixel three-dimensional imaging with time-based depth resolution," *Nature Commun.*, vol. 7, 2016, Art. no. 12010.
[25] L. You *et al.*, "Jitter analysis of a superconducting nanowire single photon detector," *AIP Adv.*, vol. 3, no. 7, 2013, Art. no. 072135.
[26] R. E. Warburton *et al.*, "Subcentimeter depth resolution using a single-photon counting time-of-flight laser ranging system at 1550 nm wavelength," *Opt. Lett.*, vol. 32, no. 15, pp. 2266–2268, 2007.
[27] A. McCarthy, R. J. Collins, N. J. Krichel, V. Fernández, A. M. Wallace, and G. S. Buller, "Long-range time-of-flight scanning sensor based on high-speed time-correlated single-photon counting," *Appl. Opt.*, vol. 48, no. 32, pp. 6241–6251, 2009.
[28] S. Chen *et al.*, "Time-of-flight laser ranging and imaging at 1550 nm using low-jitter superconducting nanowire single-photon detection system," *Appl. Opt.*, vol. 52, no. 14, pp. 3241–3245, 2013.
[29] H. Zhou *et al.*, "Few-photon imaging at 1550 nm using a low-timing-jitter superconducting nanowire single-photon detector," *Opt. Exp.*, vol. 23, no. 11, pp. 14603–14611, 2015.
[30] S. Chen *et al.*, "Dark counts of superconducting nanowire single-photon detector under illumination," *Opt. Exp.*, vol. 23, no. 8, pp. 10786–10793, 2015.